Aranda-Iglesias, D., Vadillo, G. y Rodríguez-Martínez, J.A. (2015). Constitutive sensitivity of the oscillatory behaviour of hyperelastic cylindrical shells. J*ournal of Sound and Vibration*, 358, pp. 199-216.

DOI: https://doi.org/10.1016/j.jsv.2015.07.031

Constitutive sensitivity of the oscillatory behaviour of hyperelastic cylindrical shells

D. Aranda-Iglesias, G. Vadillo, J.A. Rodríguez-Martínez *

Department of Continuum Mechanics and Structural Analysis, University Carlos III of Madrid, Avda. de la Universidad 30, 28911 Leganés, Madrid, Spain

a b s t r a c t

Free and forced nonlinear radial oscillations of a thick-walled cylindrical shell are investigated. The shell material is taken to be incompressible and isotropic within the framework of finite nonlinear elasticity. In comparison with previous seminal works dealing with the dynamic behaviour of hyperelastic cylindrical tubes, in this paper we have developed a broader analysis on the constitutive sensitivity of the oscillatory response of the shell. In this regard, our investigation is inspired by the recent works of Bucchi and Hearn (2013) [28,29], who carried out a constitutive sensitivity analysis of similar problem with hyperelastic cylindrical membranes subjected to static inflation. In the present paper we consider two different Helmholtz free-energy functions to describe the material behaviour: Mooney–Rivlin and Yeoh constitutive models. We carry out a systematic comparison of the results obtained by application of both constitutive models, paying specific attention to the critical initial and loading conditions which preclude the oscillatory response of the cylindrical tube. It has been found that these critical conditions are strongly dependent on the specific constitutive model selected, even though both Helmholtz free-energy functions were calibrated using the same experimental data.

1. Introduction

The analysis of the dynamic behaviour of incompressible hyperelastic shells aroused the interest of the scientific community thanks to the pioneering works of Knowles [1,2]. In these papers Knowles investigated, for the first time, the large-amplitude radial oscillations of a very long, thick-walled cylindrical tube. Namely, the problem of arbitrary amplitude free oscillations was considered in [1] and the problem of forced oscillations with Heaviside step pressure boundary condition was explored in [2]. Shortly after, Zhong-Heng and Soleki [3] inspected the large amplitude vibrations of thick-walled spherical hyperelastic incompressible bodies. The work of Zhong-Heng and Soleki [3] was later revisited, and adapted to the thin-walled spherical shell by Wang [4].

In any of these seminal works, due to the incompressibility of the material, the problem at hand was reduced to that of an autonomous motion of a system with a single degree of freedom. Thus, the emphasis of Knowles [1,2], Zhong-Heng and Soleki [3] and Wang [4] was on obtaining exact expressions for the period of oscillations while, due to the severe (geometrical and material) nonlinearity of these problems [5], the actual states of strain and stress were not determined. Significant efforts were made over the following years to get rid of this incompleteness and provide a full description of the

* Corresponding author. Tel.: +34 916248460; fax: +34 916249430.
E-mail address: jarmarti@ing.uc3m.es (J.A. Rodríguez-Martínez).

stress, strain and displacement fields of the problems at hand. In this regard, it is worth mentioning the work of Nowinski and Wang [6] and the series of papers by Shahinpoor and co-workers [5,7–10] that were focused on obtaining complete solutions for the full set of field variables involved in these problems. The great interest raised during the 60s and 70s by the nonlinear oscillations of hyperelastic shells has continued to the present, as detailed in the recent review of Alijani and Amabili [11].

Thus, in recent years, we have to emphasize the contributions of Beatty [12,13], Verron et al. [14,15] and Humphrey and co-workers [16,17] who investigated the radial oscillations of thick- and thin-walled cylindrical and spherical shells subjected to dynamic inflation. The loss of oscillatory behaviour was identified as a key factor which limits the capacity of hyperelastic shells for withstanding large deformations under dynamic loading. Uncovering the causes which lead to the loss of oscillatory behaviour of this type of structures is a crucial issue for different applications. For instance, the dynamic inflation of hyperelastic shells has been lately revisited with the aim of understanding the growth and rupture of arteries and aneurysms [18,19] or to develop electro-mechanical actuators that may be used as reciprocating and peristaltic pumps [20].

All these authors that are cited in previous paragraphs have raised (at least up to some extent) the key role played by the constitutive model in the dynamic response of the hyperelastic shells, and specifically in the critical conditions which lead to the loss of oscillatory behaviour of the structure. In this regard, we have to mention the latest works of Gonçalves et al. [21] and Soares and Gonçalves [22,23] who made a thorough investigation of the nonlinear vibrations of circular, annular and rectangular hyperelastic membranes. The authors showed the constitutive sensitivity of these problems using different strain energy functions calibrated with the same experimental results. In the words of Soares and Gonçalves [23] *the choice of an appropriate constitutive law is a key step in the mathematical modelling of hyperelastic materials*. This statement is further supported by Selvadurai [24] who studied the role played by the constitutive model on the deflection of hyperelastic membranes. Selvadurai [24] concluded that the selection of an appropriate (accurate) strain energy function becomes especially relevant when the objective is to model the large strain behaviour of hyperelastic solids. Moreover, this conclusion is in line with the main outcome derived from the work of Lacarbonara et al. [25] who showed the key role played by the material nonlinearity in the flexural vibrations of elastic rings. In addition, Antman and Lacarbonara [26] and Lacarbonara and Antman [27] have shown the critical influence that material compressibility and viscosity have on the radial motions of cylindrical and spherical shells.

Thus, moved by these works which pointed out the constitutive sensitivity of the oscillatory behaviour of hyperelastic shells, in this investigation we revisit the original problem of Knowles [1,2] and consider free and forced radial oscillations of cylindrical incompressible hyperelastic tubes. Two constitutive models, Mooney–Rivlin and Yeoh, calibrated with the same set of experimental data (see [28,29]) are taken into consideration. A methodical confrontation of the results obtained from both constitutive models raises their influence on the dynamic response of the cylindrical shell. Thus, we have obtained the initial, loading and geometrical conditions which, depending on the constitutive model, impede the oscillatory response of the shell. In addition, for the specific cases in which the shell shows periodic motion we have explored the influence of the constitutive model in the amplitude and period of the oscillations. Further, a complete description of the strain field of the shell is provided for selected loading cases. The salient feature of this paper is to develop an extensive and meticulous investigation to show the constitutive sensitivity of the oscillatory response of hyperelastic cylindrical shells to the full extent.

2. Problem formulation

In this section we derive the differential equations of motion describing the radial oscillations (of large amplitude) of a thick-walled cylindrical shell. The shell material is taken to be incompressible and isotropic within the framework of finite nonlinear elasticity. The main features of the mathematical derivation are presented, while further details can be found in the seminal works of Knowles [1,2].

Let (R_i, R_o) and (r_i, r_o) denote the inner and outer radii of the tube in the undeformed configuration and in the deformed configuration, respectively. Let $\{R, \Theta, Z\}$ denote the coordinates of a point in the tube in the undeformed state with reference to a fixed cylindrical coordinate system coaxial with the cylinder. A particle that was at $\{R, \Theta, Z\}$ in the undeformed state is assumed to have cylindrical coordinates $\{r(R, t), \theta, z\}$ at time t. Plane strain is considered (cylindrical shell of infinite length) and thus $z=Z$. The conservation of linear momentum in the radial direction leads to

$$\frac{\partial \sigma_r}{\partial r}+\frac{\sigma_r-\sigma_\theta}{r}=\rho \ddot{r} \tag{1}$$

where σ_r and $\sigma_\theta=\sigma$ are the radial and circumferential Cauchy stresses respectively, ρ is the material density and a superposed dot denotes differentiation with respect to time. In this work we identify the following dimensionless variables:

$$\tau=\frac{t}{t_0},\quad \overline{\sigma}_r=\frac{\sigma_r}{C_{M1}},\quad \overline{\sigma}=\frac{\sigma}{C_{M1}},\quad \overline{R}=\frac{R}{R_i},\quad \overline{r}=\frac{r}{R_i}$$

where $t_0=R_i\sqrt{\rho/C_{M1}}$, with C_{M1} being a material constant as further discussed in Section 3. Thus, Eq. (1) takes the following non-dimensional form:

$$\frac{\partial \overline{\sigma}_r}{\partial \overline{r}}+\frac{\overline{\sigma}_r-\overline{\sigma}}{\overline{r}}=\ddot{\overline{r}} \tag{2}$$

where now a superposed dot denotes differentiation with respect to the dimensionless variable τ.

Let $\lambda_r = \partial\overline{r}/\partial\overline{R}$ and $\lambda_\theta = \lambda = \overline{r}/\overline{R}$ denote the radial and circumferential stretches respectively. The stretch in the longitudinal direction is $\lambda_z = 1$ since plane strain is considered. The incompressibility condition $\lambda_r\lambda = 1$ implies that $\overline{r}^2 - \overline{r}_i^2 = \overline{R}^2 - 1$. This expression can be rewritten as

$$\overline{R}^2\left(\lambda^2 - 1\right) = \left(\lambda_i^2 - 1\right) \tag{3}$$

where $\lambda_i = \lambda_i(\tau) \equiv \overline{r}_i(\tau)$ is the circumferential stretch in the inner surface of the tube. To be noted that the motion of every material point along the thickness is determined if $\lambda_i(\tau)$ is known. Moreover, Eq. (3) allows us to express the circumferential stretch as

$$\lambda = \left(\frac{\lambda_i^2 - 1}{\overline{R}^2} + 1\right)^{1/2} \tag{4}$$

we take the derivative of Eq. (4) with respect to $\overline{R}$ to obtain the following relation:

$$\frac{\partial\lambda}{\partial\overline{R}} = -\frac{\lambda^2 - 1}{\lambda\overline{R}} \tag{5}$$

the incompressibility condition leads to $(\partial\overline{r}/\partial\overline{R})(\overline{r}/\overline{R}) = 1$, which allows us to rewrite previous expression as

$$\frac{\partial\overline{r}}{\partial\lambda} = -\frac{\overline{R}}{\lambda^2 - 1} \tag{6}$$

Inserting Eq. (6) into Eq. (2) allows us to obtain the following expression:

$$\frac{\mathrm{d}\overline{\sigma}_r}{\mathrm{d}\lambda} - \frac{\overline{\sigma}_r - \overline{\sigma}}{\lambda(\lambda^2 - 1)} = -\overline{R}^2\frac{\ddot{\lambda}}{(\lambda^2 - 1)} \tag{7}$$

Next, we take the second derivative of Eq. (4) with respect to time, which allows us to obtain the relation between $\ddot{\lambda}$ and λ:

$$\ddot{\lambda} = \frac{\lambda^2 - 1}{\lambda_i^2 - 1}\left(\frac{\dot{\lambda}_i^2 + \lambda_i\ddot{\lambda}_i}{\lambda} - \frac{\lambda_i^2\dot{\lambda}_i^2}{\lambda_i^2 - 1}\frac{\lambda^2 - 1}{\lambda^3}\right) \tag{8}$$

For a cylindrical shell of infinite length we have (see, e.g., [30])

$$\overline{\sigma}_r - \overline{\sigma} = -\lambda\frac{\mathrm{d}\overline{\psi}}{\mathrm{d}\lambda} \tag{9}$$

where the dimensionless Helmholtz free-energy function is defined as $\overline{\psi} = \psi/C_{M1}$. The specific form of ψ will be defined in Section 3.

We insert Eqs. (8) and (9) into Eq. (7), and the resulting expression is integrated over the thickness:

$$\int_{-\overline{P}_i}^{-\overline{P}_o}\mathrm{d}\overline{\sigma}_r = -\left(\lambda_i\ddot{\lambda}_i + \dot{\lambda}_i^2\right)\int_{\lambda_i}^{\lambda_o}\frac{\mathrm{d}\lambda}{\lambda(\lambda^2 - 1)} + \frac{\lambda_i^2\dot{\lambda}_i^2}{\lambda_i^2 - 1}\int_{\lambda_i}^{\lambda_o}\lambda^{-3}\,\mathrm{d}\lambda - \int_{\lambda_i}^{\lambda_o}\frac{\mathrm{d}\overline{\psi}}{\mathrm{d}\lambda}\frac{\mathrm{d}\lambda}{\lambda^2 - 1} \tag{10}$$

where $\overline{P}_i$ and $\overline{P}_o$ stand for the external pressures acting on the inner and outer surfaces of the tube (assumed time-independent), respectively and $\lambda_o = \left((\lambda_i^2 + \mu)/(1 + \mu)\right)^{1/2}$ is the circumferential stretch in the outer surface of the cylinder. Then, we obtain

$$2\Delta\overline{P} = \lambda_i\ddot{\lambda}_i\ln\left[1 + \frac{\mu}{\lambda_i^2}\right] + \dot{\lambda}_i^2\left(\ln\left[1 + \frac{\mu}{\lambda_i^2}\right] - \frac{\mu}{\mu + \lambda_i^2}\right) - 2\int_{\lambda_i}^{\lambda_o}\frac{\mathrm{d}\overline{\psi}}{\mathrm{d}\lambda}\frac{\mathrm{d}\lambda}{\lambda^2 - 1} \tag{11}$$

which is a second-order ordinary differential equation in λ_i, where $\Delta\overline{P} = \overline{P}_i - \overline{P}_o$ and $\mu = \overline{R}_o^2 - 1$ is a dimensionless parameter which represents the thickness (geometry) of the tube. Note that as μ increases the thickness of the tube increases. Upon multiplication by λ_i, previous expression assumes the next form:

$$2\lambda_i\Delta\overline{P} = q(\lambda_i)\ddot{\lambda}_i + \frac{1}{2}\frac{\mathrm{d}q(\lambda_i)}{\mathrm{d}\lambda_i}\dot{\lambda}_i^2 + \lambda_i f(\lambda_i) \tag{12}$$

where the following functions have been used:

$$q(\lambda_i) = \lambda_i^2\ln\left[1 + \frac{\mu}{\lambda_i^2}\right] \tag{13a}$$

$$f(\lambda_i) = -2\int_{\lambda_i}^{\lambda_o}\frac{\mathrm{d}\overline{\psi}}{\mathrm{d}\lambda}\frac{\mathrm{d}\lambda}{\lambda^2 - 1} \tag{13b}$$

We rearrange Eq. (12) to obtain

$$2\lambda_i \Delta\overline{P} = \frac{\mathrm{d}}{\mathrm{d}\lambda_i}\left(\frac{1}{2}q(\lambda_i)\dot{\lambda}_i^2\right) + \lambda_i f(\lambda_i) \tag{14}$$

which can be integrated twice. The first integral delivers, after some rearrangement, the so-called *energy equation* or Hamiltonian:

$$C = \tfrac{1}{2}q(\lambda_i)\dot{\lambda}_i^2 - G(\lambda_i) + F(\lambda_i) \tag{15}$$

where C is the total energy of the system $C = \frac{1}{2}q(\lambda_{i0})\dot{\lambda}_{i0}^2 - G(\lambda_{i0}) + F(\lambda_{i0})$ determined by the initial conditions, $\lambda_i(0) = \lambda_{i0}$ and $\dot{\lambda}_i(0) = \dot{\lambda}_{i0}$, as described by Knowles [1]. In this paper C will be usually referred to as the initial conditions parameter. Moreover, $\frac{1}{2}q(\lambda_i)\dot{\lambda}_i^2$ is the kinetic energy of the system, $G(\lambda_i) = 2\Delta\overline{P}\int_1^{\lambda_i}\xi\,\mathrm{d}\xi$ accounts for the work done by the external pressure and $F(\lambda_i) = \int_1^{\lambda_i}\xi f(\xi)\,\mathrm{d}\xi$ is the elastic stored energy which depends on the specific Helmholtz free-energy function selected.

From Eq. (15) the particle velocity function (phase diagram) is obtained:

$$\dot{\lambda}_i(\lambda_i) = \pm\sqrt{\frac{2(C + G(\lambda_i) - F(\lambda_i))}{q(\lambda_i)}} \tag{16}$$

To be noted that the motion is periodic if the expression $C + G(\lambda_i) - F(\lambda_i)$ has *at least* two real roots. A second integration of Eq. (14) provides the temporal behaviour of the circumferential stretch:

$$\tau(\lambda_i) = \pm\int \frac{\mathrm{d}\lambda_i}{\dot{\lambda}_i(\lambda_i)} \tag{17}$$

To be noted that when the motion of the shell is periodic (further discussions about the oscillatory response of the shell are presented in Sections 4 and 5), the corresponding phase curve is a closed loop in the $\dot{\lambda}(\lambda)$ plane. Then, the period T can be calculated as

$$T(\lambda_i) = 2\int_a^b \frac{\mathrm{d}\lambda_i}{\dot{\lambda}_i(\lambda_i)} \tag{18}$$

with a and b being the two real roots that define the oscillatory behaviour of the material. The inversion of Eq. (18) to obtain the temporal evolution of the circumferential stretch in the inner surface $\lambda_i(\tau)$ requires numerical integration. Once the motion is completely determined the radial, circumferential and longitudinal stresses $\{\sigma_r, \sigma_\theta, \sigma_z\}$ are obtained by direct application of the specific Helmholtz free-energy function selected (Section 3).

3. Constitutive modelling

Two different Helmholtz free-energy functions are taken to describe the material behaviour: Mooney–Rivlin and Yeoh constitutive models.

- Mooney–Rivlin

$$\psi = C_{M1}(I_1 - 3) + C_{M2}(I_2 - 3) \tag{19}$$

where $I_1 = \lambda_r^2 + \lambda_\theta^2 + \lambda_z^2$ and $I_2 = \lambda_r^2\lambda_\theta^2 + \lambda_\theta^2\lambda_z^2 + \lambda_r^2\lambda_z^2$ are the first and second invariants of the Green strain tensor, respectively. Moreover, C_{M1} and C_{M2} are material constants. To be noted that C_{M1} is the material constant used in Section 2 to pose the problem in non-dimensional form.

- Yeoh

$$\psi = C_{Y1}(I_1 - 3) + C_{Y2}(I_1 - 3)^2 + C_{Y3}(I_1 - 3)^3 \tag{20}$$

where C_{Y1}, C_{Y2} and C_{Y3} are material constants. As stated by Boyce and Arruda [31] and Selvadurai [24], the specific goal of the high order I_1 terms in the Yeoh model is to capture the response of hyperelastic materials at large strains.

These strain–energy functions are frequently used to describe the behaviour of rubber like materials [14,32–34]. The parameters values (given in Appendix A) are taken from Bucchi and Hearn [29], where the same set of experimental results [32] was used to calibrate the models. These two constitutive models are selected because they have distinct functional dependencies of λ on ψ, which allows us to expose the constitutive sensitivity of the oscillatory behaviour of thick-walled cylindrical shells. The high order I_1 terms in the formulation of the Yeoh model are mainly responsible for the substantial differences in the predictions obtained from these two strain energy functions in Sections 4 and 5. Moreover, the reader is referred to the works of Boyce and Arruda [31], Saccomandi and Ogden [35] and Selvadurai [24] for in-depth reviews of the constitutive models proposed over the last decades to describe hyperelastic responses of rubber-like materials.

In Section 4 we investigate the case of free oscillations, which allows us to determine the role played by initial conditions in the oscillatory motion of the shell. In Section 5 we investigate the case of forced oscillations, which is suitable to analyse

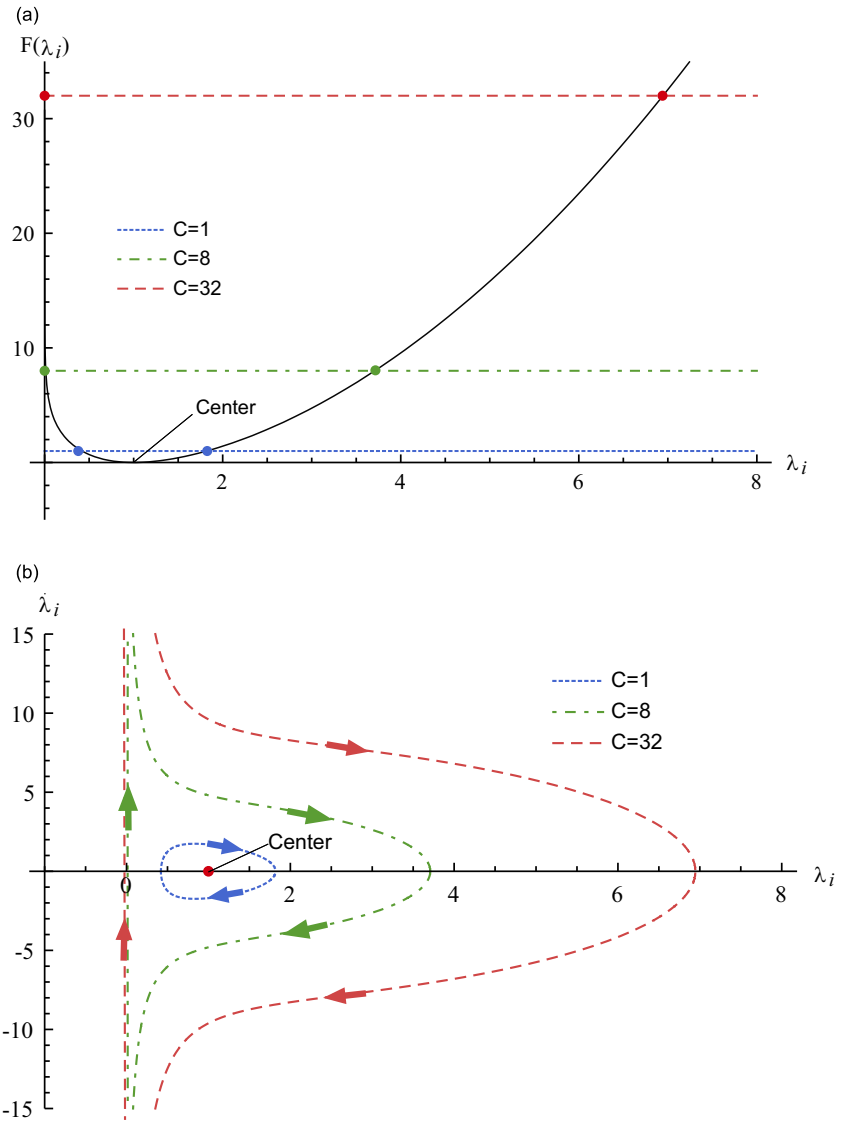

Fig. 1. Free oscillations. Mooney–Rivlin constitutive model. The thickness parameter is $\mu = 1$. Three values of the initial conditions parameter are investigated: $C=1$, $C=8$ and $C=32$. (a) Elastic stored energy $F(\lambda_i)$ versus stretch λ_i. (b) Phase diagram, $\dot{\lambda}_i$ versus λ_i.

the role played by loading pressure in the oscillatory motion of the shell. All along Sections 4 and 5 we present a systematic confrontation of the results obtained using Mooney–Rivlin and Yeoh constitutive models.

4. Analysis and results: free oscillations

Free oscillations implies that $\Delta\overline{P} = 0$ and therefore $G(\lambda_i) = 0$ and $G(\lambda_{i0}) = 0$. Then, Eqs. (16) and (18) become

$$\dot{\lambda}_i(\lambda_i) = \pm\sqrt{\frac{2(C - F(\lambda_i))}{q(\lambda_i)}} \tag{21a}$$

$$T(\lambda_i) = 2\int_a^b \sqrt{\frac{q(\lambda_i)}{2(C - F(\lambda_i))}}\,\mathrm{d}\lambda_i \tag{21b}$$

As anticipated in Section 2, for the motion to be periodic is required that the expression $C - F(\lambda_i)$ has at least two real roots. Next, we explore the existence of these *two roots* for both constitutive models and different initial conditions.

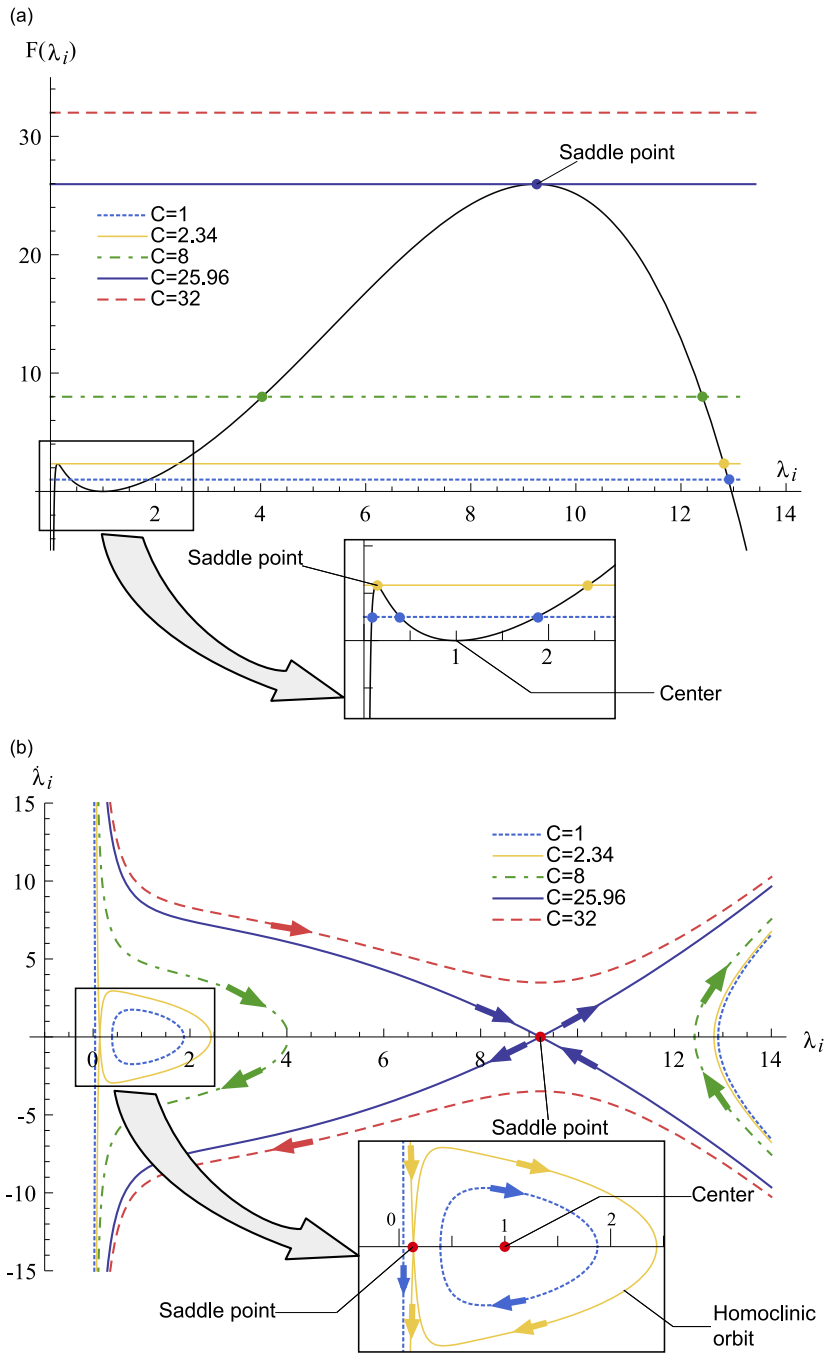

Fig. 2. Free oscillations. Yeoh constitutive model. The thickness parameter is $\mu = 1$. Five values of the initial conditions parameter are investigated: $C=1$, $C=2.34$, $C=8$, $C=25.96$ and $C=32$. (a) Elastic stored energy $F(\lambda_i)$ versus stretch λ_i. (b) Phase diagram, $\dot{\lambda}_i$ versus λ_i.

4.1. Influence of the initial conditions

Fig. 1(a) shows, for the Mooney–Rivlin constitutive model, the elastic stored energy $F(\lambda_i)$ versus the stretch λ_i. The thickness parameter is taken to be $\mu = 1$ (from now on, the reference value). The stored energy is zero for $\lambda_i = 1$. $F(\lambda_i)$ decreases monotonically within the range $0 < \lambda_i < 1$ and increases monotonically for $\lambda_i > 1$. Note that the general shape of the function $F(\lambda_i)$ does not depend on μ. Nevertheless, decreasing μ flattens the $F(\lambda_i)$ curve. Three values of the initial conditions parameter are depicted (horizontal lines): $C=1$ (reference value), $C=8$ and $C=32$. The motion is only possible within the regions in which $F(\lambda_i)$ lies below the selected value of C. The vertical distance between the corresponding value of C and the function $F(\lambda_i)$ determines the kinetic energy of the system. Fig. 1(b) shows the phase diagram for the initial

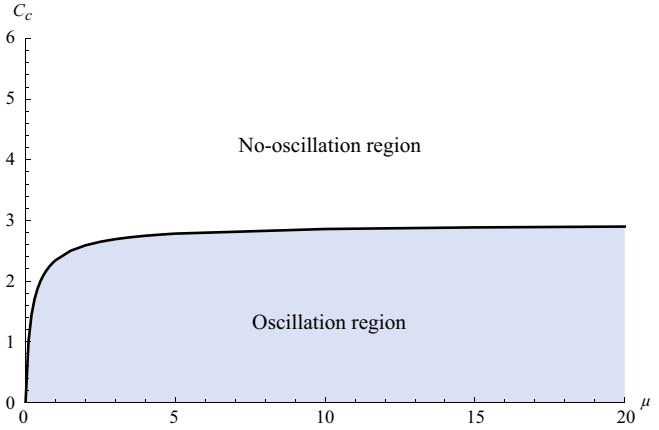

Fig. 3. Free oscillations. Yeoh constitutive model. Critical initial conditions for oscillatory response of the cylindrical shell C_c as a function of the geometrical parameter μ.

conditions parameters illustrated in Fig. 1(a). For the three values of C investigated the phase diagram is a closed loop. This implies that the motion of the cylindrical shell is periodic. The first intersection of the $(\dot{\lambda}_i, \lambda_i)$ trajectory with the λ_i-axis (first root of the expression $C - F(\lambda_i)$) occurs within the range $0 < \lambda_i < 1$ and the second intersection for $\lambda_i > 1$. As C increases, the energy of the system is greater, which boosts the amplitude of the oscillations and the velocity of the shell during the oscillations.

Fig. 2(a) shows, for the Yeoh constitutive model, the elastic stored energy $F(\lambda_i)$ versus the stretch λ_i. The thickness parameter is $\mu = 1$. $F(\lambda_i)$ neither decreases monotonically within the range $0 < \lambda_i < 1$ nor increases monotonically for $\lambda_i > 1$. The curve $F(\lambda_i)$–λ_i shows a relative maximum (finite and positive) within the range $0 < \lambda_i < 1$ and an absolute maximum (finite and positive) for $\lambda_i > 1$. Note that, when μ tends to zero (membrane hypothesis), both maximums tend to the same value of $F(\lambda_i)$. Five initial conditions are considered: $C=1$, $C=2.34$, $C=8$, $C=25.96$ and $C=32$. Each value of C provides a different number of roots in the expression $C - F(\lambda_i)$. This leads to five different *scenarios* in the phase plane shown in Fig. 2(b):

- $C=1$: The expression $C - F(\lambda_i)$ has four real roots. In Fig. 2(b) is shown that the first intersection with the λ_i-axis occurs for $\lambda_i \approx 0.08$ and corresponds to an open curve, i.e. non-oscillatory motion. The second and third intersections occur for $\lambda_i \approx 0.38$ and $\lambda_i \approx 1.87$ respectively. These two real roots define a closed loop in the phase plane, i.e. oscillatory motion. The fourth intersection is located at $\lambda_i \approx 12.93$ and corresponds to an open curve.
- $C=2.34$: The expression $C - F(\lambda_i)$ has three real roots. This value of C determines the limit of the oscillatory behaviour (the horizontal line passes through the local maximum). A closed (homoclinic) trajectory is defined by the first root (saddle point) located at $\lambda_i \approx 0.15$ and the second root of $C - F(\lambda_i)$ located at $\lambda_i \approx 2.43$. The third root is found for $\lambda_i \approx 12.81$ and corresponds to an open trajectory.
- $C=8$: The expression $C - F(\lambda_i)$ has two real roots. Both of them correspond to open curves. For this value of the parameter C the cylindrical shell does not oscillate. The first intersection with the λ_i-axis is located at $\lambda_i \approx 3.99$ and the second one at $\lambda_i \approx 12.43$.
- $C=25.96$: The expression $C - F(\lambda_i)$ has one single root (saddle point), which belongs simultaneously to two different open trajectories. This root corresponds to the absolute maximum of the curve shown in Fig. 2(a), which is located at $\lambda_i \approx 9.24$. For this value of the parameter C the cylindrical shell does not oscillate.
- $C=32$: The expression $C - F(\lambda_i)$ has no real roots, as shown in Fig. 2(a). For this value of the parameter C the cylinder does not oscillate.

Depending on the initial conditions, the solution may oscillate around the center or grow exponentially away from the saddle point. Following Verron et al. [14] this is considered a kind of *escape from a potential well* phenomenon which is frequently observed in Hamiltonian systems [36]. Moreover, one should note that, when μ tends to zero, it is possible to find a value of the initial conditions such that C will intersect both maximums of the function $F(\lambda_i)$. This specific case will lead to a heteroclinic orbit in the phase plane.

In Fig. 2 we showed that 2.34 is the maximum value of C for which the Yeoh shell may oscillate. Nevertheless, this maximum value of C (from now on referred to as the critical initial conditions C_c) depends on the thickness of the cylinder. Fig. 3 shows the critical initial conditions C_c versus the geometrical parameter μ. For small values of μ the value of C_c rapidly increases with increasing thickness of the cylinder. For large values of μ the critical initial conditions are largely independent of the thickness of the cylinder and $C_c \approx 2.9$.

Next, we pay attention to the specific cases for which the response of the cylinder is oscillatory. In Fig. 4 we show the period of the oscillation T versus the parameter C for Mooney–Rivlin and Yeoh constitutive models. The reference value $\mu = 1$ is taken:

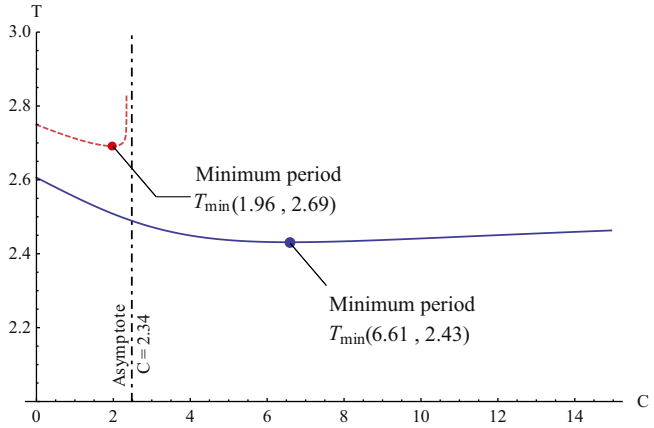

Fig. 4. Free oscillations. Period of the oscillation T versus the initial conditions parameter C for Mooney–Rivlin (solid line) and Yeoh (dashed line) constitutive models. The reference value $\mu = 1$ is taken.

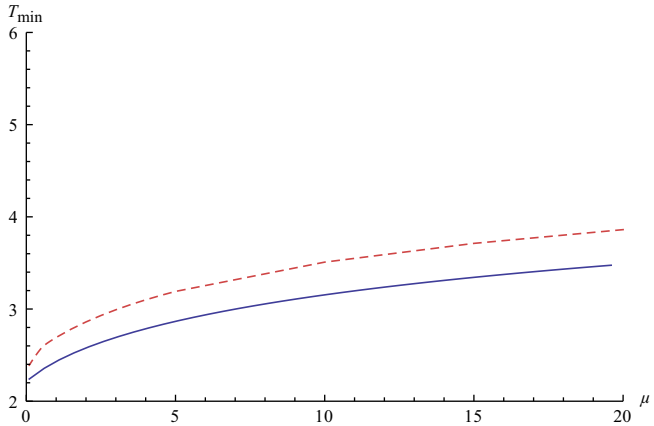

Fig. 5. Free oscillations. Minimum period T_{min} versus the geometrical parameter μ for Mooney–Rivlin (solid line) and Yeoh (dashed line) constitutive models.

- Mooney–Rivlin: The period decreases monotonically for $C \lesssim 6.61$, reaches a minimum denoted by T_{min} at $C \approx 6.61$ and then increases. Large values of C are accompanied by a decrease of the influence that the initial conditions have on the value of T. For sufficiently large values of C we have checked that the period becomes rather independent of C such that $T \approx 2.60$.
- Yeoh: The period decreases monotonically for $C \lesssim 1.96$, reaches a minimum at $C \approx 1.96$ and then increases, tending asymptotically to infinity for $C = 2.34$ (homoclinic trajectory). To be noted that the value of C associated to T_{min} is much smaller in the case of the Yeoh material. Moreover, note that the T–C curve runs above the Mooney–Rivlin one, i.e. the oscillations are shorter-in-time in the case of the Mooney–Rivlin constitutive model.

Let us focus on the minimum of the T–C curves, which determines the shortest-in-time oscillations for a given geometry. This minimum varies with the geometrical parameter μ. Fig. 5 shows the minimum period T_{min} versus the thickness parameter μ for both Mooney–Rivlin and Yeoh materials. Irrespective of the constitutive model considered, the minimum period of the oscillations increases with the thickness of the shell. The T_{min}–μ curves for Mooney–Rivlin and Yeoh models evolve (almost) parallel, being the results obtained for the Yeoh material always above.

4.2. Temporal behaviour of the circumferential stretch

For selected initial conditions, we investigate the temporal behaviour of the circumferential stretch in the inner surface of the shell. This is obtained after inversion and subsequent numerical integration of Eq. (17).

Fig. 6 shows λ_i versus τ for both constitutive models investigated and two different initial conditions: $C = 1$, $\lambda_{i0} = 1$ and $\dot{\lambda}_{i0} = 1.698$ in Fig. 6(a); $C = 32$, $\lambda_{i0} = 1$ and $\dot{\lambda}_{i0} = 9.608$ in Fig. 6(b). For $C = 1$ we have an oscillatory response of the shell for both constitutive models. It is shown that the amplitude and the period of the oscillation are slightly larger in the case of the Yeoh material, as anticipated in Figs. 1(b), 2(b) and 4. The maximum and the minimum of the λ_i–τ curve are 1.87 and 0.38 for the Yeoh model, 1.81 and 0.41 for the Mooney–Rivlin, respectively. For $C = 32$ the response of the Mooney–Rivlin is periodic, whereas the response of the Yeoh is not. To be noted that the predictions of both material models practically overlap up to

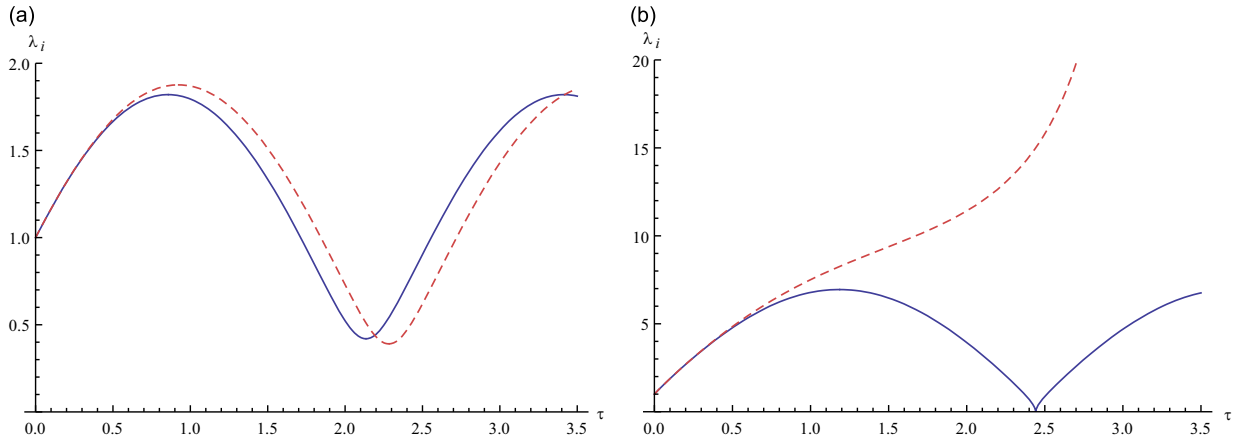

Fig. 6. Free oscillations. Circumferential stretch in the inner surface of the shell λ_i versus dimensionless time τ for Mooney–Rivlin (solid line) and Yeoh (dashed line) constitutive models. The reference value $\mu = 1$ is taken. (a) $C = 1$, $\lambda_{i0} = 1$ and $\dot{\lambda}_{i0} = 1.698$. (b) $C = 32$, $\lambda_{i0} = 1$ and $\dot{\lambda}_{i0} = 9.608$.

$\tau \approx 0.5$, this loading time determines the onset of *noticeable discrepancies* between both constitutive models. For $\tau \gtrsim 0.5$ the Mooney–Rivlin model predicts an oscillatory response of the circumferential stretch which is characteristic of periodic motion, while the Yeoh model shows a monotonic increase of λ_i with τ which represents a continuous radial expansion of the cylindrical shell.

If the initial conditions are such that the response of the shell is oscillatory for both constitutive equations investigated, these models predict stretch fields that are rather similar. Interestingly, it is possible to find initial conditions for which the response of the shell is strongly dependent on the constitutive model, to an extent that the Mooney–Rivlin material predicts oscillatory motion while the Yeoh material predicts an unbounded expansion (or contraction) of the cylinder. In this regard it is worth mentioning that, for design purposes, the Yeoh constitutive model provides *more conservative predictions* than the Mooney–Rivlin.

5. Analysis and results: forced oscillations

In this section we will raise the case of radial oscillations due to suddenly applied constant pressures on lateral surfaces. The shell is taken to be initially in equilibrium and unstretched, $\lambda_{i0} = 1$ and $\dot{\lambda}_{i0} = 0$, which leads to $C = 0$. This facilitates to investigate the role played by the applied pressure in the dynamic response of the cylindrical shell. Eqs. (16) and (18) now take the form

$$\dot{\lambda}_i(\lambda_i) = \pm \sqrt{\frac{2\left(G(\lambda_i) - F(\lambda_i)\right)}{q(\lambda_i)}} \tag{22a}$$

$$T(\lambda_i) = 2\int_a^b \sqrt{\frac{q(\lambda_i)}{2\left(G(\lambda_i) - F(\lambda_i)\right)}}\, \mathrm{d}\lambda_i \tag{22b}$$

where $G(\lambda_i) = \left(1 - \lambda_i^2\right)\Delta\overline{P}$ irrespective of the constitutive model selected. Note that $F(\lambda_i) - G(\lambda_i)$ represents the potential energy of the system. As stated in Section 2, for the motion to be periodic it is required that the expression $G(\lambda_i) - F(\lambda_i)$ has at least two real roots. One of these roots is imposed by the initial conditions ($\lambda_{i0} = 1$). The existence of additional real roots will determine whether the motion of the shell may be periodic or not. Next, we explore the existence of these *additional roots* for both constitutive models and different applied pressures.

5.1. Influence of the loading pressure

- Mooney–Rivlin: We have that

$$F(\lambda_i) = K\left(1 - \lambda_i^2\right)\ln\left(\frac{1 + \mu/\lambda_i^2}{1 + \mu}\right)$$

where $K = 1 - C_{M2}/C_{M1}$. Then, the real roots of the expression $G(\lambda_i) - F(\lambda_i)$ are calculated

$$a = 1; \quad b = \sqrt{\frac{\mu}{(1+\mu)\exp\left(-\Delta\overline{P}/K\right) - 1}}$$

as anticipated, the first root corresponds to the initial conditions. The second root gives the maximum circumferential stretch that can be reached (for a given applied pressure) during the periodic motion.

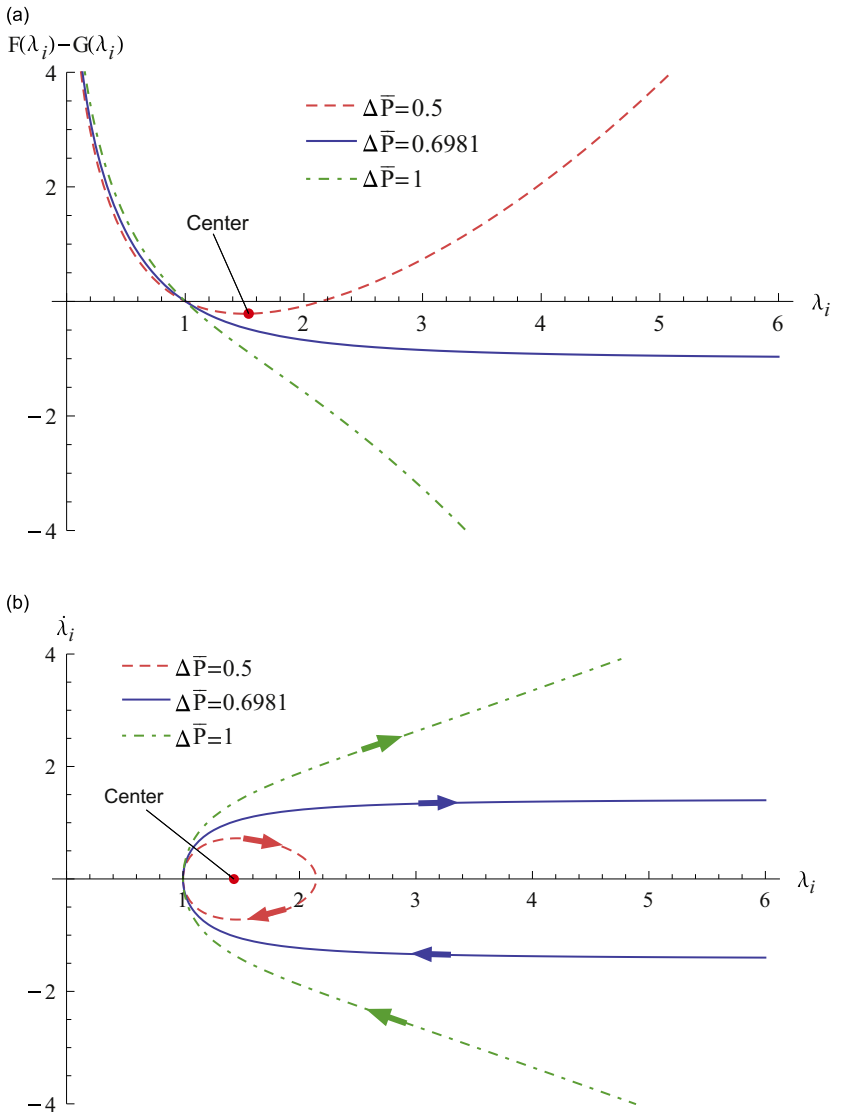

Fig. 7. Forced oscillations. Mooney–Rivlin constitutive model. The thickness parameter is $\mu = 1$. Three values of the applied pressure are investigated: $\Delta\overline{P} = 0.5$, $\Delta\overline{P} = 0.6981$ and $\Delta\overline{P} = 1$. (a) Potential energy $F(\lambda_i) - G(\lambda_i)$ versus stretch λ_i. (b) Phase diagram, $\dot{\lambda}_i$ versus λ_i.

For $\Delta\overline{P} < 0$ the expression which defines the critical negative pressure $\Delta\overline{P}_{c^-}$ for which the shell shows oscillatory behaviour is

$$\Delta\overline{P}_{c^-} = \lim_{\lambda_i \to 0} K \ln\left(\frac{1+\mu}{1+\mu/\lambda_i^2}\right) = -\infty \tag{23}$$

which reveals that the motion is periodic irrespective of the negative pressure applied.
For $\Delta\overline{P} > 0$ the expression which defines the critical positive pressure $\Delta\overline{P}_{c^+}$ for which the shell shows oscillatory behaviour is

$$\Delta\overline{P}_{c^+} = \lim_{\lambda_i \to \infty} K \ln\left(\frac{1+\mu}{1+\mu/\lambda_i^2}\right) = K \ln(1+\mu) \tag{24}$$

which reveals that there is a limit in applied pressure for which the response of the shell is oscillatory. This limiting positive pressure depends on the thickness of the cylindrical tube by the parameter μ. Hereinafter, for the Mooney–Rivlin material, we will specifically focus on positive applied pressures to analyse the critical conditions of oscillation. Fig. 7 shows the potential energy of the system $F(\lambda_i) - G(\lambda_i)$ versus the stretch λ_i and the phase plane for three different positive applied pressures: $\Delta\overline{P} = 0.5$, $\Delta\overline{P} = 0.6981$ and $\Delta\overline{P} = 1$. Each selected value of $\Delta\overline{P}$ defines a different *scenario* in the phase plane. The reference geometrical parameter $\mu = 1$ is considered. Irrespective of the applied pressure, the first

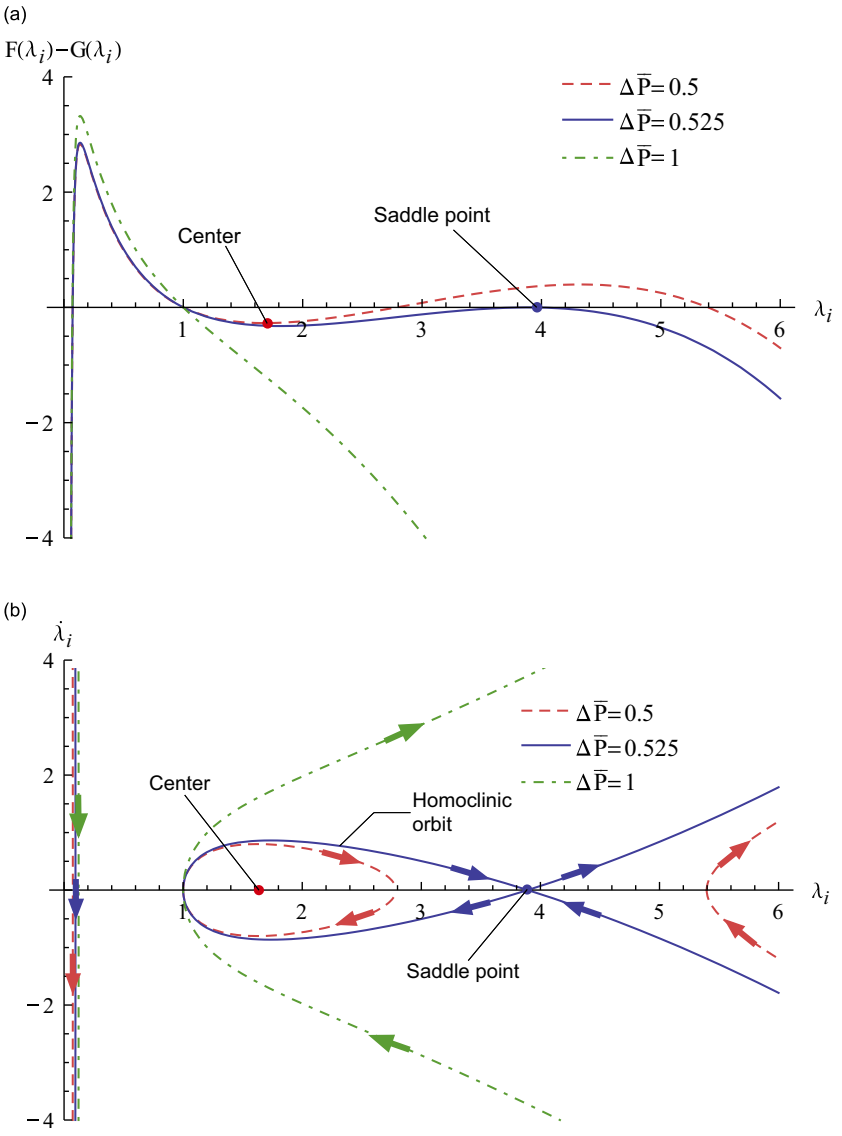

Fig. 8. Forced oscillations. Yeoh constitutive model. The thickness parameter is $\mu = 1$. Three values of the applied pressure are investigated: $\Delta\overline{P} = 0.5$, $\Delta\overline{P} = 0.525$ and $\Delta\overline{P} = 1$. (a) Potential energy $F(\lambda_i) - G(\lambda_i)$ versus stretch λ_i. (b) Phase diagram, $\dot{\lambda}_i$ versus λ_i.

real root of the expression $G(\lambda_i) - F(\lambda_i)$ is found for $\lambda_i = 1$ (as imposed by the initial conditions). This corresponds with an intersection of the phase curves with the λ_i–axis. Whenever the expression $G(\lambda_i) - F(\lambda_i)$ has a second root, the phase curve will be a closed trajectory in the $\left(\dot{\lambda}_i, \lambda_i\right)$ plane.

- $\Delta\overline{P} = 0.5$: We have that $\Delta\overline{P} < \Delta\overline{P}_{c^+}$ and the expression $G(\lambda_i) - F(\lambda_i)$ has a second real root located at $\lambda_i = 2.13$. The corresponding $\dot{\lambda}_i$–λ_i curve is a closed loop in the phase plane.
- $\Delta\overline{P} = 0.6981$: The critical pressure $\Delta\overline{P}_{c^+}$ is reached. For large values of λ_i the potential energy $F(\lambda_i) - G(\lambda_i)$ becomes an horizontal asymptote. The corresponding phase trajectory shows a second intersection with the λ_i-axis for $\lambda_i \to \infty$.
- $\Delta\overline{P} = 1$: We have that $\Delta\overline{P} > \Delta\overline{P}_{c^+}$ and the expression $G(\lambda_i) - F(\lambda_i)$ does not have a second real root. The potential energy decreases monotonically for $\lambda_i > 1$ and the corresponding trajectory is an open curve in the phase plane.

- Yeoh: We have that

$$F(\lambda_i) = \left(\lambda_i^2 - 1\right)\left[\frac{C_{Y3}}{C_{M1}}\ \frac{2\lambda_i^6 - 6\lambda_i^2 + 1}{2\lambda_i^4} + \frac{(\mu+1)^2(6\lambda_i^2 + 6\mu - 1) - 2(\lambda_i^2 + \mu)^3}{2(\lambda_i^2 + \mu)(\mu+1)}\right)$$
$$+ \frac{C_{Y2}}{C_{M1}}\ \frac{\lambda_i^4 - 1}{\lambda_i^2} + \frac{(\mu+1)^2 - (\lambda_i^2 + \mu)^2}{(\lambda_i^2 + \mu)(\mu+1)}\Bigg) + \frac{3C_{Y3} + 2C_{Y2} + C_{Y1}}{C_{M1}} \ln\frac{\lambda_i^2 + \mu}{(\mu+1)\lambda_i^2}\Bigg] \tag{25}$$

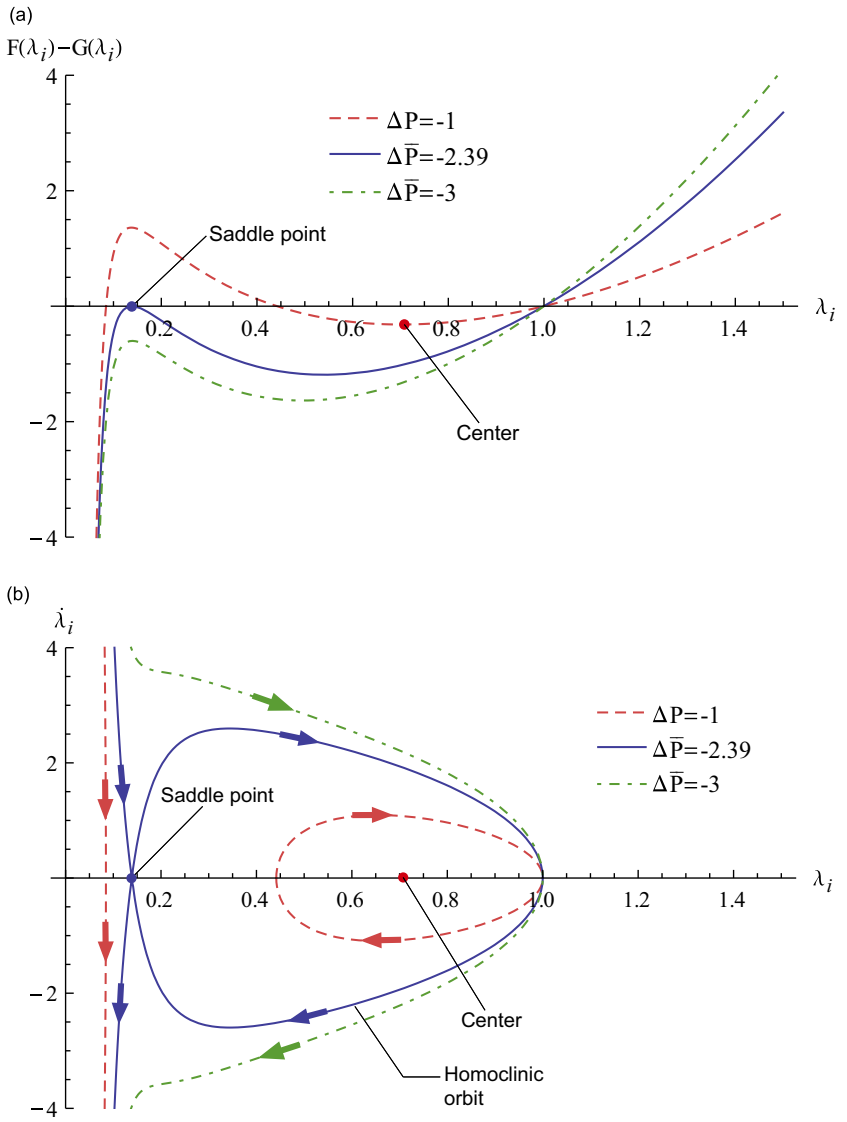

Fig. 9. Forced oscillations. Yeoh constitutive model. The thickness parameter is $\mu = 1$. Three values of the applied pressure are investigated: $\Delta\overline{P} = -1$, $\Delta\overline{P} = -2.39$ and $\Delta\overline{P} = -3$. (a) Potential energy $F(\lambda_i) - G(\lambda_i)$ versus stretch λ_i. (b) Phase diagram, $\dot{\lambda}_i$ versus λ_i.

As anticipated, $\lambda_i = 1$ is a root of the expression $G(\lambda_i) - F(\lambda_i)$. Additional real roots have to be calculated numerically. Unlike the results obtained for the Mooney–Rivlin material, application of negative pressures does not ensure the periodic response of the cylindrical shell. We find numerically that, for $\mu = 1$, the critical positive and negative pressures to ensure oscillatory behaviour are $\Delta\overline{P}_{c^+} = 0.525$ and $\Delta\overline{P}_{c^-} = -2.39$ respectively.

Fig. 8 shows the potential energy of the system $F(\lambda_i) - G(\lambda_i)$ versus the stretch λ_i and the phase plane for three different positive applied pressures: $\Delta\overline{P} = 0.5$, $\Delta\overline{P} = 0.525$ and $\Delta\overline{P} = 1$. Each selected value of $\Delta\overline{P}$ defines a different *scenario* in the phase plane. The reference geometrical parameter $\mu = 1$ is considered.

- $\Delta\overline{P} = 0.5$: We have that $\Delta\overline{P} < \Delta\overline{P}_{c^+}$. The expression $G(\lambda_i) - F(\lambda_i)$ has four real roots. The first intersection of the potential energy with the λ_i-axis occurs for $\lambda_i \approx 0.08$. This root corresponds to an open curve. The second intersection occurs for $\lambda_i = 1$ (due to the imposed initial conditions) and the third one for $\lambda_i = 2.77$. These two real roots define a closed loop in the phase plane. The fourth intersection is located at $\lambda_i \approx 5.4$ and corresponds to an open curve.
- $\Delta\overline{P} = 0.525$: We have that $\Delta\overline{P} = \Delta\overline{P}_{c^+}$. This value of $\Delta\overline{P}$ determines the limit of the oscillatory behaviour. The expression $G(\lambda_i) - F(\lambda_i)$ has three real roots. The first one is found for $\lambda_i \approx 0.08$ and defines an open trajectory in the phase plane. The second root is located at $\lambda_i = 1$ and the third one at $\lambda_i \approx 3.89$ (saddle point). These two roots define a closed (homoclinic) trajectory in the phase space.

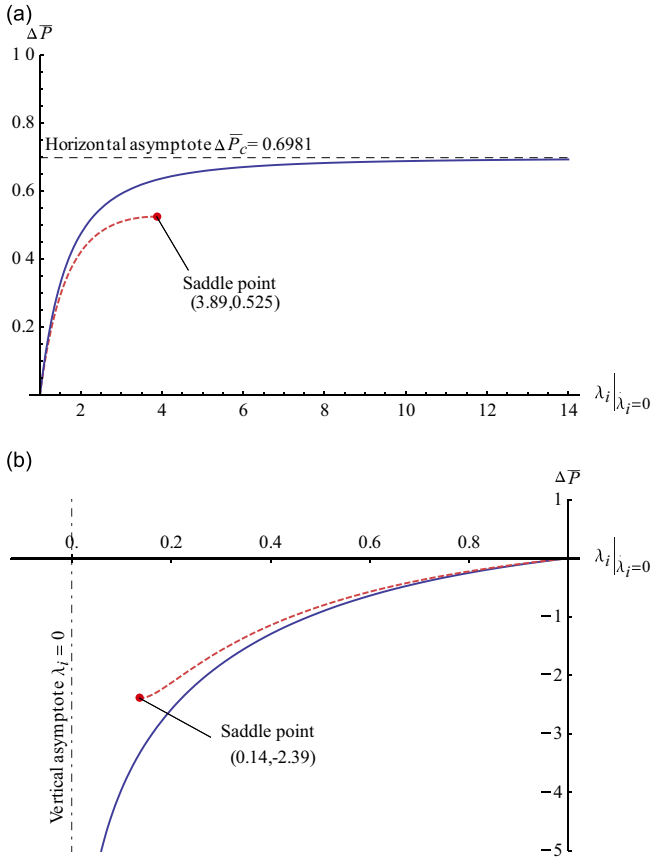

Fig. 10. Forced oscillations. Applied pressure $\Delta\overline{P}$ versus the maximum stretch of the oscillation $\lambda_i|_{\dot{\lambda}_i=0}$ for Mooney–Rivlin (solid line) and Yeoh (dashed line) constitutive models. (a) Positive applied pressure and (b) negative applied pressure.

- $\Delta\overline{P}=1$: We have that $\Delta\overline{P}>\Delta\overline{P}_{c^+}$. The expression $G(\lambda_i)-F(\lambda_i)$ has two real roots. The first intersection with the λ_i-axis is located at $\lambda_i\approx 0.08$ and the second one at $\lambda_i=1$. Both roots define open curves in the phase plane. For this value of $\Delta\overline{P}$ the cylindrical shell does not oscillate.

Fig. 9 shows the potential energy of the system $F(\lambda_i)-G(\lambda_i)$ versus the stretch λ_i and the phase plane for three different negative applied pressures: $\Delta\overline{P}=-1$, $\Delta\overline{P}=-2.39$ and $\Delta\overline{P}=-3$. Each value of $\Delta\overline{P}$ defines a different *scenario* in the phase plane. We have taken $\mu=1$.

- $\Delta\overline{P}=-1$: We have that $\Delta\overline{P}<\Delta\overline{P}_{c^-}$. The expression $G(\lambda_i)-F(\lambda_i)$ has four roots located at $\lambda_i\approx 0.08, 0.44, 1, 20.8$. The first one and the last one define open trajectories in the phase space. Note that, for the sake of clarity, the fourth root is not shown in the graph. The second and third roots define a closed loop in the phase plane.
- $\Delta\overline{P}=-2.39$: We have that $\Delta\overline{P}=\Delta\overline{P}_{c^-}$. This value of $\Delta\overline{P}$ determines the limit of the oscillatory behaviour. The expression $G(\lambda_i)-F(\lambda_i)$ has three real roots. The first one (saddle point) is located at $\lambda_i=0.14$ and the second one at $\lambda_i=1$. These two roots define a closed (homoclinic) trajectory in the phase diagram. The third root is located at $\lambda_i=28.8$ and defines an open trajectory in the phase space. For the sake of clarity, this is not shown in the graph.
- $\Delta\overline{P}=-3$: We have that $\Delta\overline{P}>\Delta\overline{P}_{c^-}$. The expression $G(\lambda_i)-F(\lambda_i)$ has two roots. The first one is located at $\lambda_i=1$ and the second one at $\lambda_i=31$. The latter is not shown in the graph for the sake of clarity. Both roots define open trajectories in the phase plane. For this value of $\Delta\overline{P}$ the cylindrical shell does not oscillate.

Note that, for any of the loading cases discussed above, the trajectories which do not pass through the coordinates (1,0) of the phase plane do not have physical meaning since they do not satisfy the initial conditions that we have imposed.

Next, we focus the attention in the cases for which the response of the cylinder is oscillatory. Fig. 10 shows the applied pressure $\Delta\overline{P}$ versus the maximum stretch of the oscillation $\lambda_i|_{\dot{\lambda}_i=0}$ for both constitutive models investigated and $\mu=1$.

Fig. 10(a) illustrates the results obtained for positive applied pressures. For the Mooney–Rivlin material the curve shows a power-type concave down shape, the maximum stretch of the oscillation $\lambda_i|_{\dot{\lambda}_i=0}$ increases nonlinearly with the applied

pressure $\Delta\overline{P}$. On the one hand the values of $\lambda_i|_{\dot{\lambda}_i=0}$ are very modest for short values of $\Delta\overline{P}$. On the other hand $\lambda_i|_{\dot{\lambda}_i=0}$ tends to infinity for $\Delta\overline{P}=0.6981$. This means that, virtually, the Mooney–Rivlin material may show oscillations of infinite amplitude. As for the Mooney–Rivlin model, the curve obtained for the Yeoh material shows a power-type concave down shape which extends up to $\lambda_i|_{\dot{\lambda}_i=0}=3.89$. This value of the maximum stretch is reached for $\Delta\overline{P}=0.525$. Larger values of $\lambda_i|_{\dot{\lambda}_i=0}$ cannot be reached in the periodic motion of the Yeoh shell. Note that for short values of $\Delta\overline{P}$ the values of $\lambda_i|_{\dot{\lambda}_i=0}$ obtained for Mooney–Rivlin and Yeoh constitutive models are very similar. As the applied pressure increases, the difference between the predictions of both models occurs. For a given value of $\Delta\overline{P}$, the Yeoh material shows oscillations of larger amplitude.

Fig. 10(b) shows the results obtained for negative applied pressures. For the Mooney–Rivlin model the value of $\lambda_i|_{\dot{\lambda}_i=0}$ shows a monotonic nonlinear decrease with increasing (in absolute value) applied pressure such that $\lambda_i|_{\dot{\lambda}_i=0}$ tends to zero when $\Delta\overline{P}\to-\infty$. Virtually, the Mooney–Rivlin material may show oscillations of infinite amplitude. For the Yeoh constitutive model $\lambda_i|_{\dot{\lambda}_i=0}$ decreases nonlinearly with increasing pressure (in absolute value) until $\lambda_i|_{\dot{\lambda}_i=0}=0.14$. This value of the stretch is obtained for $\Delta\overline{P}=-2.39$. Smaller values of $\lambda_i|_{\dot{\lambda}_i=0}$ cannot be reached in the periodic motion of the shell. Note that for short applied pressures the values of $\lambda_i|_{\dot{\lambda}_i=0}$ obtained for Mooney–Rivlin and Yeoh constitutive models are very similar. As the applied pressure increases (in absolute value) the $\Delta\overline{P}-\lambda_i|_{\dot{\lambda}_i=0}$ curves gradually deviate from each other. For a given value of $\Delta\overline{P}$, the Yeoh material shows oscillations of larger amplitude.

It is exposed the interplay between the amplitude of the oscillations and the constitutive behaviour of the shell material. For short values of the applied pressure (whatever this is positive or negative) the amplitude of the oscillations is hardly influenced by the constitutive model selected, but large differences appear as $\Delta\overline{P}$ increases (in absolute value). Note that the Mooney–Rivlin model allows for indefinitely large amplitudes, whereas for the Yeoh model the amplitude of the oscillation is limited to finite values.

We explore below the interplay between the period of the oscillations and the constitutive behaviour of the shell. In Fig. 11 we show the period of the oscillations T versus the applied pressure $\Delta\overline{P}$ for both constitutive models investigated and $\mu=1$.

- Mooney–Rivlin: For positive applied pressures the period of the oscillations increases nonlinearly with $\Delta\overline{P}$. This increase becomes steeper with the applied pressure such that the T–$\Delta\overline{P}$ curve develops a vertical asymptote for $\Delta\overline{P}=0.6981$. This value corresponds to the maximum (positive) pressure $\Delta\overline{P}_{c^+}$ which leads to an oscillatory response of the shell. The period of the oscillations for $\Delta\overline{P}_{c^+}$ tends to infinity because the amplitude of the oscillations tends to infinity, as illustrated in Fig. 7(b). For negative applied pressures the period T smoothly and monotonically decreases with increasing (in absolute value) $\Delta\overline{P}$.
- Yeoh: The period of the oscillations increases nonlinearly with $\Delta\overline{P}$ for positive applied pressures. This increase is steeper as the critical positive pressure $\Delta\overline{P}_{c^+}$ (corresponding to $\Delta\overline{P}=0.525$) is approached. The period of the oscillations for $\Delta\overline{P}_{c^+}$ tends to infinity because a homoclinic orbit is reached, as illustrated in Fig. 8(b). For negative applied pressures the period T decreases with increasing (in absolute value) $\Delta\overline{P}$, until the critical negative value $\Delta\overline{P}_{c^-}$ is reached. Then, a homoclinic orbit is reached (see Fig. 9(b)) and the period of oscillation goes to infinity. To be highlighted that, for positive applied pressures, increasing differences between the predictions of both models are found as $\Delta\overline{P}$ increases. For negative applied pressures, within the range of applied pressures for which the Yeoh model provides predictions ($\Delta\overline{P}<\Delta\overline{P}_{c^-}$ in absolute value), the differences are negligible.

The critical values of the applied pressure for which the shell shows oscillatory motion are dependent on the geometry of the cylinder. This interplay is investigated in Fig. 12 where the critical applied pressure $\Delta\overline{P}_c$ (whatever this is positive $\Delta\overline{P}_{c^+}$ or negative $\Delta\overline{P}_{c^-}$) is depicted versus the geometrical parameter μ for Mooney–Rivlin and Yeoh constitutive models.

- Mooney–Rivlin: The critical positive applied pressure increases monotonically (and nonlinearly) with the geometrical parameter μ. As the thickness of the shell increases, the pressure required to induce a non-oscillatory response of the cylinder increases. Recall that – for the Mooney–Rivlin material – the shell shows periodic motion no matter the value of the negative pressure applied, i.e. there is not critical negative applied pressure.
- Yeoh: The critical positive applied pressure increases monotonically with the geometrical parameter μ. Note that the $\Delta\overline{P}_{c^+}$–μ curve runs always below the Mooney–Rivlin. The difference between the predictions of both constitutive models increases with μ. Unlike the Mooney–Rivlin constitutive model, the Yeoh predicts a critical negative pressure which increases (in absolute value) with μ. This increase is very sharp for short values of μ but it gets rapidly reduced as μ increases. Interestingly, for sufficiently large values of μ, the critical negative pressure becomes largely independent of the thickness of the cylinder.

5.2. Temporal behaviour of the circumferential stretch

For selected loading cases, we investigate the temporal behaviour of the circumferential stretch in the inner surface of the shell. This is obtained after inversion and subsequent numerical integration of Eq. (17).

Fig. 13 shows λ_i versus τ for both constitutive models investigated and four different applied pressures: $\Delta\overline{P}=0.5$ and $\overline{P}_o=0$ in Fig. 13(a); $\Delta\overline{P}=0.6$ and $\overline{P}_o=0$ in Fig. 13(b); $\Delta\overline{P}=-1$ and $\overline{P}_o=1$ in Fig. 13(c); $\Delta\overline{P}=-3$ and $\overline{P}_o=3$ in Fig. 13(d).

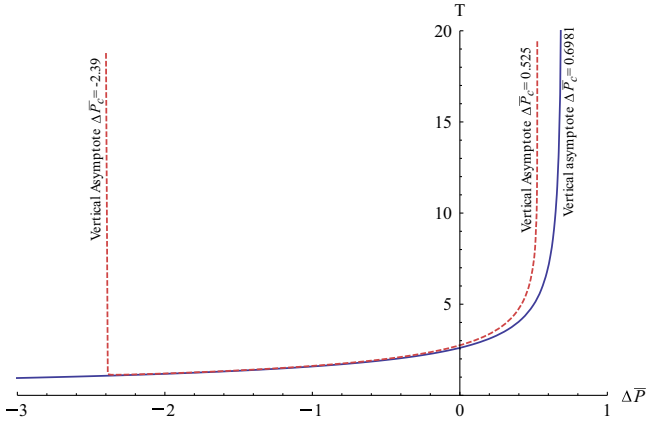

Fig. 11. Forced oscillations. Period of the oscillation T versus the applied pressure $\Delta\overline{P}$ for Mooney–Rivlin (solid line) and Yeoh (dashed line) constitutive models. The reference value $\mu = 1$ is taken.

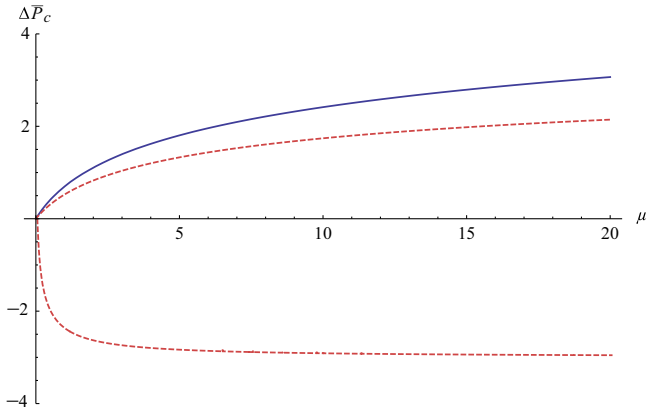

Fig. 12. Forced oscillations. Critical applied pressure $\Delta\overline{P}_c$ versus the geometrical parameter μ for Mooney–Rivlin (solid line) and Yeoh (dashed line) constitutive models.

Fig. 13(a) and (b) shows positive applied pressures. For $\Delta\overline{P} = 0.5$ both constitutive models show oscillatory behaviour. The amplitude and the period of the oscillation are larger in the case of the Yeoh material, as anticipated in Figs. 7(b), 8(b) and 11. The maximum of the λ_i–τ curve is 2.77 for the Yeoh model and 2.13 for the Mooney–Rivlin. The minimum is given by the initial condition $\lambda_i = 1$. For $\Delta\overline{P} = 0.6$ the response of the Mooney–Rivlin is periodic, whereas the response of the Yeoh is not. The predictions of both material models practically overlap up to $\tau \approx 1$. For $\tau \gtrsim 1$ the Mooney–Rivlin model shows an oscillatory response of the circumferential stretch, while the Yeoh model shows a monotonic increase of λ_i with τ which represents an unbounded radial expansion of the shell. Fig. 13(c) and (d) shows negative applied pressures. For $\Delta\overline{P} = -1$ both constitutive models show oscillatory behaviour. The amplitude, and specially the period of the oscillation, is similar for both constitutive models, as anticipated in Fig. 11. The minimum of the λ_i–τ curve is 0.44 for the Yeoh model and 0.48 for the Mooney–Rivlin. The maximum is given by the initial condition $\lambda_i = 1$. For $\Delta\overline{P} = -3$ the response of the Mooney–Rivlin is periodic, whereas the response of the Yeoh is not. The predictions of both material models practically overlap up to $\tau \approx 0.4$. For $\tau \gtrsim 0.4$ the Mooney–Rivlin model shows an oscillatory response of the circumferential stretch, while the Yeoh model shows a monotonic (and drastic) decrease of λ_i with τ which represents an unbounded radial contraction of the shell.

It is possible to find loading conditions for which the response of the shell is oscillatory if the Mooney–Rivlin model is selected and non-oscillatory if the Yeoh model is taken. This reinforces the idea introduced in Section 4 that, despite both constitutive equations are calibrated using the same experimental data [28,29], the Yeoh constitutive model provides *more conservative predictions*. This is a relevant outcome with important implications for engineering design purposes.

6. Summary and conclusions

In this paper we have studied free and forced radial oscillations of thick-walled hyperelastic cylindrical shells. The shell material has been described using Mooney–Rivlin and Yeoh constitutive models that were calibrated by Bucchi and Hearn [29] using the same experimental data. Below we show the key outcomes of this investigation:

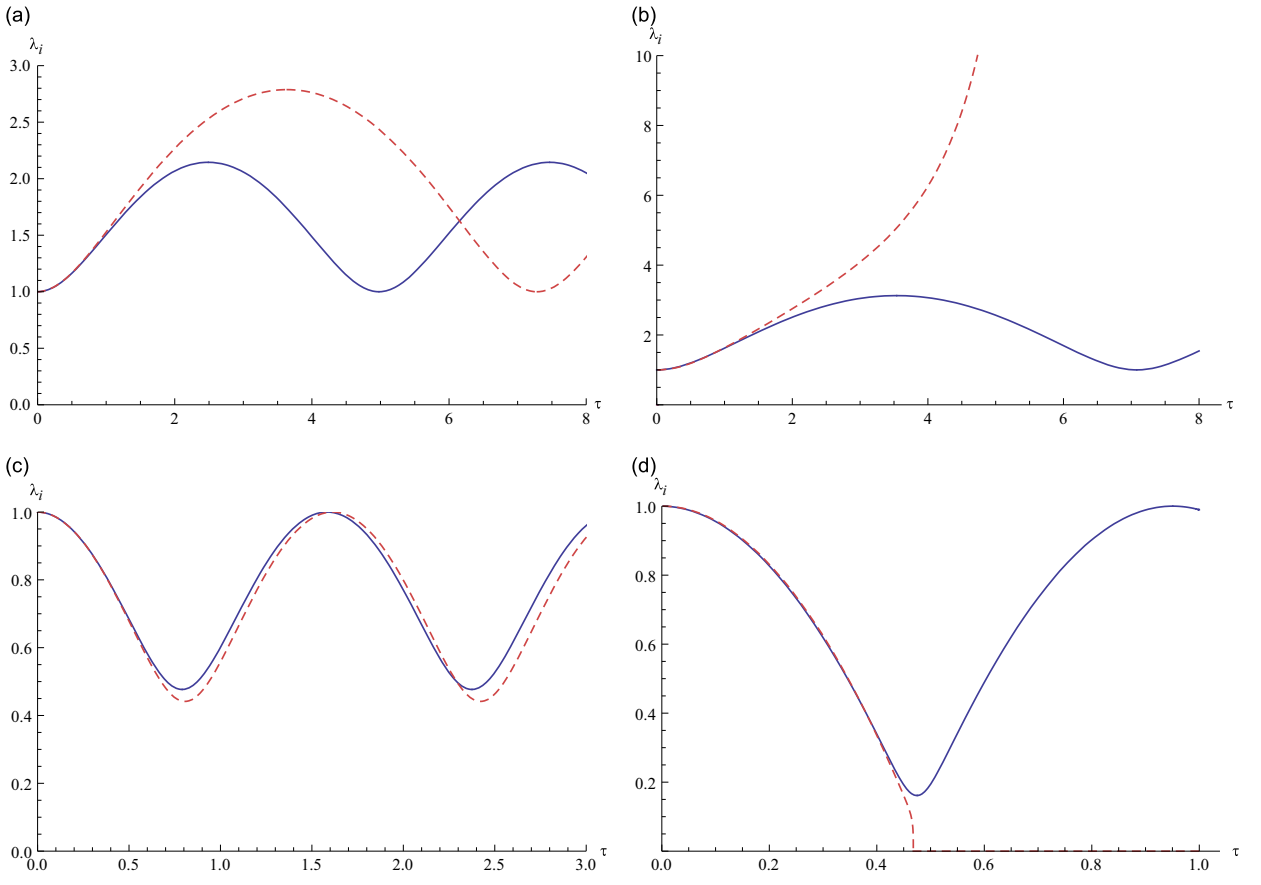

Fig. 13. Forced oscillations. Circumferential stretch in the inner surface of the shell λ_i versus dimensionless time τ for Mooney–Rivlin (solid line) and Yeoh (dashed line) constitutive models. The reference value $\mu = 1$ is taken. (a) $\Delta\overline{P} = 0.5$ and $\overline{P}_o = 0$. (b) $\Delta\overline{P} = 0.6$ and $\overline{P}_o = 0$. (c) $\Delta\overline{P} = -1$ and $\overline{P}_o = 1$. (d) $\Delta\overline{P} = -3$ and $\overline{P}_o = 3$.

Table A1
Mooney–Rivlin parameters taken from [29], Eq. (19).

Mooney–Rivlin parameters, Eq. (19)	
C_{M1} (Pa)	210 587.307
C_{M2} (Pa)	1504.76719

Table A2
Yeoh parameters taken from [29], Eq. (20).

Yeoh parameters, Eq. (20)	
C_{Y1} (Pa)	190 592.559
C_{Y2} (Pa) −	1634.89996
C_{Y3} (Pa)	41.3399927

- *Free oscillations*: Following Knowles [1] we have defined a parameter C which represents the total energy (initial conditions) of the system. We have demonstrated that the Mooney–Rivlin shell shows an oscillatory response irrespective of the value of C considered, whereas the Yeoh shell displays a non-oscillatory behaviour if C is sufficiently large. The critical value of the initial conditions which leads to unbounded expansion or contraction of the Yeoh shell is denoted by C_c and depends on the thickness of the cylindrical tube, which has been defined by the dimensionless parameter μ. The interplay between C_c and μ is such that for small values of μ the value of C_c rapidly increases with the thickness of the cylinder, whereas for large values of μ the value of C_c becomes largely independent of the thickness of the cylinder.
  Further, for the loading cases which lead to periodic motion of the cylinder, we have investigated the role played by the constitutive model in the temporal behaviour of the shell. We have shown that the period of the oscillations T is larger for the Yeoh material than for the Mooney–Rivlin, irrespective of the initial conditions considered. Moreover, we have reported that the T–C curves show a minimum denoted as $T_{\min}$ for both constitutive models, which determines the shortest-in-time oscillations for a given geometry. It has been shown that $T_{\min}$ increases as the thickness of the cylindrical tube increases.
- *Forced oscillations*: Following Knowles [2] we have defined a parameter $\Delta\overline{P}$ such that we have outward net pressure for positive $\Delta\overline{P}$ and inward net pressure for negative $\Delta\overline{P}$. The shell is taken to be initially in equilibrium and unstretched, i.e. $C=0$. We have shown that the Mooney–Rivlin shell shows an oscillatory response for $\Delta\overline{P}<0$, whereas for $\Delta\overline{P}>0$ the response of the cylinder is non-oscillatory (unbounded expansion) if the applied pressure is sufficiently large. On the contrary, the Yeoh shell shows non-oscillatory behaviour whether the outward net pressure (unbounded contraction) or the inward net pressure (unbounded expansion) is large enough. The critical value of the applied pressure, whether it is positive $\Delta\overline{P}_{c^+}$ or negative $\Delta\overline{P}_{c^-}$, which leads to non-oscillatory motion of the shell depends on the thickness of the cylindrical tube μ. For outward net pressure the value of $\Delta\overline{P}_{c^+}$ monotonically increases with μ for both constitutive models. Note that, irrespective of μ, the value of $\Delta\overline{P}_{c^+}$ is larger for the Mooney–Rivlin material than for the Yeoh. For inward net pressure (recall that only the Yeoh shell may show unbounded contraction) the value of $\Delta\overline{P}_{c^-}$ sharply increases for short values of μ but it becomes largely independent of the thickness of the cylinder for large values of μ. Besides that, for the loading cases which lead to the periodic motion of the cylinder we have explored the amplitude of the oscillations. We have shown that, irrespective of the constitutive model, the amplitude of the oscillations increases nonlinearly with the absolute value of the applied pressure. Further, we have determined that the Yeoh material shows oscillations with larger amplitude than the Mooney–Rivlin. This difference in the predictions of both constitutive models increases with the absolute value of the applied pressure $\Delta\overline{P}$. In addition, we have investigated the interplay between the applied pressure $\Delta\overline{P}$ and the period of the oscillations T. It has been shown that, irrespective of the constitutive model, the oscillations become greater (in time) with the applied pressure, being the relation between $\Delta\overline{P}$ and T highly nonlinear. Further, we have determined that for negative applied pressures $\Delta\overline{P}<0$ the period of the oscillations is very similar for Mooney–Rivlin and Yeoh constitutive models, while the difference emerges for positive applied pressures $\Delta\overline{P}>0$.

We have determined the initial, loading and geometrical (critical) conditions which, depending on the constitutive model, prevent the oscillatory response of the shell. We have found that within the oscillatory regime the response of the shell is similar for both constitutive models, while the critical conditions that lead to non-oscillatory motion are largely different. Specifically, we have determined that the Yeoh material is significantly more prone to develop an unbounded expansion/contraction, whether we consider free or forced oscillations. Within the context of engineering design, our findings serve to claim that the Yeoh constitutive model provides *more conservative predictions* than the Mooney–Rivlin. The latter material model prognosticates the loss of oscillatory behaviour of the cylindrical shell for larger values of the initial (stored and/or kinetic) energy and greater applied pressures.

Acknowledgements

The authors would like to thank Professor J. Fernández-Sáez for his helpful suggestions and discussions.

The authors are indebted to the *Ministerio de Economía y Competitividad de España* (Project DPI2014–57989–P) for the financial support which permitted to conduct this work.

Appendix A. Material parameters of the Helmholtz free-energy functions

See Tables A1 and A2.

References

[1] J.K. Knowles, Large amplitude oscillations of a tube of incompressible elastic material, *Quarterly of Applied Mathematics* 18 (1960) 71–77.
[2] J.K. Knowles, On a class of oscillations in the finite deformation theory of elasticity, *Journal of Applied Mechanics* 29 (1962) 283–286.
[3] G. Zhong-Heng, R. Soleki, Free and forced finite-amplitude oscillations of an elastic thick-walled hollow sphere made of incompressible material, *Archiwum Mechaniki Stosowanej* 15 (1963) 427–433.
[4] C.C. Wang, On the radial oscillations of a spherical thin shell in the finite elasticity theory, *Quarterly of Applied Mathematics* 23 (1965) 270–274.
[5] M. Shahinpoor, R. Balakrishnan, Large amplitude oscillations of thick hyperelastic cylindrical shells, *International Journal of Non-Linear Mechanics* 13 (1979) 295–301.
[6] J.L. Nowinski, A.S.D. Wang, Galerkin's solution to a severely non-linear problem of finite elastodynamics, *International Journal of Non-Linear Mechanics* 1 (1966) 219–228.
[7] M. Shahinpoor, J.L. Nowinski, Exact solution to the problem of forced large amplitude radial oscillations of a thin hyperelastic tube, *International Journal of Non-Linear Mechanics* 6 (1971) 193–207.
[8] M. Shahinpoor, Large amplitude oscillations of a hollow spherical dielectric, *International Journal of Non-Linear Mechanics* 7 (1972) 527–534.
[9] B. Balakrishnan, M. Shahinpoor, Finite amplitude oscillations of a thin hyperelastic spherical shell, *Iranian Journal of Science and Technology* 7 (1977) 14–20.
[10] B. Balakrishnan, M. Shahinpoor, Finite amplitude oscillations of a hyperelastic spherical cavity, *International Journal of Non-Linear Mechanics* 13 (1978) 171–176.
[11] F. Alijani, M. Amabili, Non-linear vibrations of shells: *a literature review from 2003 to 2013*, *International Journal of Non-Linear Mechanics* 58 (2014) 233–257.
[12] M.F. Beatty, Infinitesimal stability of the equilibrium states of an incompressible, isotropic elastic tube under pressure, *Journal of Elasticity* 104 (2011) 71–90.
[13] M.F. Beatty, Small amplitude radial oscillations of an incompressible isotropic elastic spherical shell, *Mathematics and Mechanics of Solids* 16 (2011) 492–512.
[14] E. Verron, R.E. Khayat, A. Derdouri, B. Peseux, Dynamic inflation of hyperelastic spherical membranes, *Journal of Rheology* 43 (1999) 1083–1097.
[15] E. Verron, G. Marckmann, B. Peseux, Dynamic inflation of non-linear elastic and viscoelastic rubber-like membranes, *International Journal for Numerical Methods in Engineering* 50 (2001) 1233–1251.
[16] A.D. Shah, J.D. Humphrey, Finite strain elastodynamics of saccular aneurysms, *Journal of Biomechanics* 32 (1999) 593–599.
[17] G. David, J.D. Humphrey, Further evidence for the dynamic stability of intracranial saccular aneurysms, *Journal of Biomechanics* 36 (2003) 1143–1150.
[18] H. Haslach, J. Humphrey, Dynamics of biological soft tissue and rubber: *internally pressurized spherical membranes surrounded by a fluid*, *International Journal of Non-Linear Mechanics* 39 (2004) 399–420.
[19] A. Samuelson, P. Seshaiyer, Stability of membrane elastodynamics with applications to cylindrical aneurysms, *Journal of Applied Mathematics* 2011 (2011).
[20] E.M. Mockensturm, N. Goulbourne, Dynamic response of dielectric elastomers, *International Journal of Non-Linear Mechanics* 41 (2006) 388–395.
[21] P.B. Gonçalves, R.M. Soares, D. Pamplona, Nonlinear vibrations of a radially stretched circular hyperelastic membrane, *Journal of Sound and Vibration* 327 (2009) 231–248.
[22] R.M. Soares, P.B. Gonçalves, Nonlinear vibrations and instabilities of a stretched hyperelastic annular membrane, *International Journal of Solids and Structures* 49 (2012) 514–526.
[23] R.M. Soares, P.B. Gonçalves, Large-amplitude nonlinear vibrations of a Mooney–Rivlin rectangular membrane, *Journal of Sound and Vibration* 333 (2014) 2920–2935.
[24] A.P.S. Selvadurai, Deflections of a rubber membrane, *Journal of the Mechanics and Physics of Solids* 54 (2006) 1093–1119.
[25] W. Lacarbonara, A. Arena, S.S. Antman, Flexural vibrations of nonlinearly elastic circular rings, *Meccanica* 50 (2015) 689–705.
[26] S.S. Antman, W. Lacarbonara, Forced radial motions of nonlinearly viscoelastic shells, *Journal of Elasticity* 96 (2009) 155–190.
[27] W. Lacarbonara, S.S. Antman, Parametric instabilities of the radial motions of non-linearly viscoelastic shells under pulsating pressures, *International Journal of Non-Linear Mechanics* 47 (2012) 461–472.
[28] A. Bucchi, E.H. Hearn, Predictions of aneurysm formation in distensible tubes: *Part A—theoretical background to alternative approaches*, *International Journal of Mechanical Sciences* 71 (2013) 1–20.
[29] A. Bucchi, E.H. Hearn, Predictions of aneurysm formation in distensible tubes: *Part B—application and comparison of alternative approaches*, *International Journal of Mechanical Sciences* 70 (2013) 155–170.
[30] R.W. Ogden, *Non-Linear Elastic Deformations*, Dover Publications, Mineola, NY, 1997.
[31] M.C. Boyce, E.M. Arruda, Constitutive models for rubber elasticity: *a review*, *Rubber Chemistry and Technology* 73 (2000) 504–523.
[32] L.R.G. Treolar, Stress–strain data for vulcanised rubber under various types of deformation, *Transactions of the Faraday Society* 40 (1944) 59–70.
[33] L.R.G. Treolar, *The Physics of Rubber Elasticity*, Clarendon Press, Oxford, UK, 1949.
[34] O.H. Yeoh, Some forms of the strain–energy function for rubber, *Rubber Chemistry and Technology* 66 (1993) 754–771.
[35] G. Saccomandi, R.W. Ogden, *Mechanics and Thermomechanics of Rubberlike Solids, CISM Courses and Lectures no. 452*, Springer, Wien, 2004.
[36] J. Guckenheimer, P. Holmes, *Nonlinear Oscillations, Dynamical Systems, and Bifurcation of Vector Fields*, Springer, New York ed., 1983.